energies

MDPI

Article

Multi-Objective Optimization Strategy for Permanent Magnet Synchronous Motor Based on Combined Surrogate Model and Optimization Algorithm

Yinquan Yu [1,2,3,*], Yue Pan [1,2,3], Qiping Chen [1,2,3], Yiming Hu [1,2,3], Jian Gao [4], Zhao Zhao [5], Shuangxia Niu [6] and Shaowei Zhou [7]

1 School of Mechatronics and Vehicle Engineering, East China Jiaotong University, Nanchang 330013, China
2 Key Laboratory of Conveyance and Equipment of Ministry of Education, East China Jiaotong University, Nanchang 330013, China
3 Institute of Precision Machining and Intelligent Equipment Manufacturing, East China Jiaotong University, Nanchang 330013, China
4 School of Electrical and Information Engineering, Hunan University, Changsha 410006, China
5 Faculty of Electrical Engineering and Information Technology, Otto-von-Guericke University of Magdeburg, 39106 Magdeburg, Germany
6 Department of Electrical Engineering, The Hong Kong Polytechnic University, Hong Kong 999077, China
7 CRRC Changchun Railway Vehicles Corporation Limited, 435 Qingyin Road, Changchun 130062, China
* Correspondence: yinquan.yu@gmail.com

Abstract: When a permanent magnet synchronous motor (PMSM) is designed according to the traditional motor design theory, the performance of the motor is often challenging to achieve the desired goal, and further optimization of the motor design parameters is usually required. However, the motor is a strongly coupled, non-linear, multivariate complex system, and it is a challenge to optimize the motor by traditional optimization methods. It needs to rely on reliable surrogate models and optimization algorithms to improve the performance of the PMSM, which is one of the problematic aspects of motor optimization. Therefore, this paper proposes a strategy based on a combination of a high-precision combined surrogate model and the optimization method to optimize the stator and rotor structures of interior PMSM (IPMSM). First, the variables were classified into two layers with high and low sensitivity based on the comprehensive parameter sensitivity analysis. Then, Latin hypercube sampling (LHS) is used to obtain sample points for highly sensitive variables, and various methods are employed to construct surrogate models for variables. Each optimization target is based on the acquired sample points, from which the most accurate combined surrogate model is selected and combined with non-dominated ranking genetic algorithm-II (NSGA-II) to find the best. After optimizing the high-sensitivity variables, a new finite element model (FEM) is built, and the Taguchi method is used to optimize the low-sensitivity variables. Finally, finite element analysis (FEA) was adopted to compare the performance of the initial model and the optimized ones of the IPMSM. The results showed that the performance of the optimized motor is improved to prove the effectiveness and reliability of the proposed method.

Keywords: IPMSM; sensitivity analysis; surrogate model; Taguchi method

Citation: Yu, Y.; Pan, Y.; Chen, Q.; Hu, Y.; Gao, J.; Zhao, Z.; Niu, S.; Zhou, S. Multi-Objective Optimization Strategy for Permanent Magnet Synchronous Motor Based on Combined Surrogate Model and Optimization Algorithm. *Energies* **2023**, *16*, 1630. https://doi.org/10.3390/en16041630

Academic Editor: Gianluca Brando

Received: 19 December 2022
Revised: 10 January 2023
Accepted: 2 February 2023
Published: 6 February 2023

1. Introduction

Due to its high power factor, high torque density, high efficiency, high reliability, and other advantages, PMSM is widely used in electric vehicles, aerospace, and other vital fields [1–3]. To design an efficient and reliable PMSM, the researchers optimized both the controller and the body structure of the PMSM. The structure optimization of the PMSM is mainly divided into single-objective optimization [4,5] and multi-objective optimization [6–26] of the motor. Traditional single-objective optimization methods often consider only individual motor performance. In contrast, the overall performance of the

PMSM is affected by output torque, torque ripple, speed range, loss, temperature rise, and many other factors. In [4,5], a method for effectively weakening the tooth groove torque of the motor is proposed; however, other performance indicators, such as average torque, loss, efficiency, etc., are not taken into account. Although this single-objective optimization method can significantly improve the particular performance index of the motor, it is always premised on sacrificing other performances of the motor, which is not conducive to the overall performance improvement of the PMSM. Therefore, the current PMSM optimization study is mainly a multi-objective optimization method. In the literature [6–8], the parametric scanning method is applied to optimize the performance of the motor. This method can effectively find out the combination of design variables that meet the objective conditions, but this process requires much computation, is very time-consuming, and is not suitable for application in the case of many design variables. In order to reduce the computation time, in the literature [9–11], the Taguchi method is introduced to optimize the objective performance of the motor. This method finds the best combination of design variables based on orthogonal test design and analysis. It can effectively optimize the performance of the motor with fewer trials, and the optimization efficiency is high. Therefore, the Taguchi method is often used by designers to optimize the design of mechanical structures. However, in the case of large value ranges of design variables, the Taguchi method has a large span of adjacent value levels in the design space, and many high-quality design variables will be ignored. The optimization accuracy is insufficient. To overcome this difficulty, in the literature [12,13], the combination of fuzzy theory and the Taguchi method is introduced to convert multiple objectives to a single objective and update the value ranges of design variables in the optimization process based on the sequential Taguchi method, and then again optimize the performance of the IPMSM, thereby effectively improving the optimization accuracy. However, this method requires much manual calculation with complicated data processing.

To further improve the multi-objective optimization effect of the PMSM, in addition to the aforementioned Taguchi method, the response surface method [14,15], and the intelligent optimization algorithm [17–25], other methods are also applied in the optimization design of the motor and provide more optimization solutions to improve the performance of the motor. In the literature [14,15], the response surface method is adopted to obtain the non-linear relationship between variables and objectives and perform a comprehensive analysis to obtain the best combination of design variables of the performance of the motor. The motor optimization design based on the intelligent optimization algorithm is mainly used to build the surrogate model and then be combined with the optimization algorithm to look for the combination of variables that meet the requirements [16]. The surrogate models commonly used in optimization problems of the PMSM are the response surface method (RSM) model [17], the Kriging model [18], the support vector regression (SVR) model [19], etc. The reliability of the whole optimization is directly determined by the goodness of the surrogate model. If the surrogate model does not accurately reflect the mapping relationship between the design variables and the optimization objectives, even if it is combined with the optimization algorithm, it cannot produce accurate and effective results. The optimization algorithms commonly used in optimizing the PMSM are genetic algorithms [20], particle swarm algorithms [21], etc. In the literature [22], radial basis function (RBF) neural network and multi-island genetic algorithm (MIGA) are combined for the torque performance optimization of the motor. In the literature [23], the average torque, the torque ripple, the average suspension force, and the suspension force ripple of the motor are taken as the optimization objectives. In the optimization process, the combination of RSM and improved MOPSO is adopted. The results show that the torque Performance of the motor is improved. However, the RSM usually uses the relationship between the second-order polynomial fitting variables and the objective performance. The fitting accuracy cannot be guaranteed to be high enough when there are many variables. In the literature [24], to obtain a more accurate approximation relationship between the design variables and the optimization objectives, a variety of different surrogate models are established, analyzed,

and compared. The best-performing random forest (RF) surrogate model is selected to optimize the performance indicators of the motor in combination with NSGA-II. Although the surrogate model combined with the intelligent optimization algorithm can effectively obtain the optimal combination of design variables in the optimization design of the PMSM, as the number of design variables increases, the accuracy of the surrogate model decreases, and the convergence of the optimization algorithm is more difficult. It is a challenge to obtain the optimal value. In this case, the optimization strategy of the PMSM is very critical. By taking into account many design variables [25], the sensitivity analysis method can be used to divide the design variables into two layers of sensitivity and insensitivity and then optimize them, respectively. The results show that this strategy can effectively solve the optimization problem of many design variables. However, in that paper, only the torque performance of the motor is considered. In the literature [26], a strategy for optimizing the structure of the IPM motor based on deep learning is proposed. The process trains the model by inputting a cross-sectional image of the rotor structure of the motor and the corresponding output performance data. Then it selects the best combination of design variables based on the trained model. However, the data samples required by the method are too large, and the technique is very time-consuming.

In this paper, a multi-objective optimization strategy based on a combined surrogate model and the optimization algorithm is proposed to optimize the average torque, the torque ripple, and the loss of the IPMSM. The rest of this paper is as follows: The FEM model of the IPMSM is established, and the optimization process of IPMSM is introduced in Section 2. In Section 3, the optimization variables and objectives are determined, and the optimization variables are divided into high-sensitivity variables and low-sensitivity variables according to the comprehensive sensitivity analysis. The high-sensitivity variables are optimized by using the surrogate model in combination with NSGA-II, and the low-sensitivity variables are optimized by using the Taguchi method. In Section 4, the performances of the pre-optimization and post-optimization motors are verified and contrasted. Conclusions are drawn in Section 5.

2. IPMSM Models and Optimization Process

In this paper, an IPMSM is taken as the optimization specimen. The FEM of IPMSM is shown in Figure 1a, and the main parameters of the IPMSM are shown in Table 1. The main dimensions of the motor are set within the reasonable design range, and the PMs are inserted into the V-shaped structure rotor core.

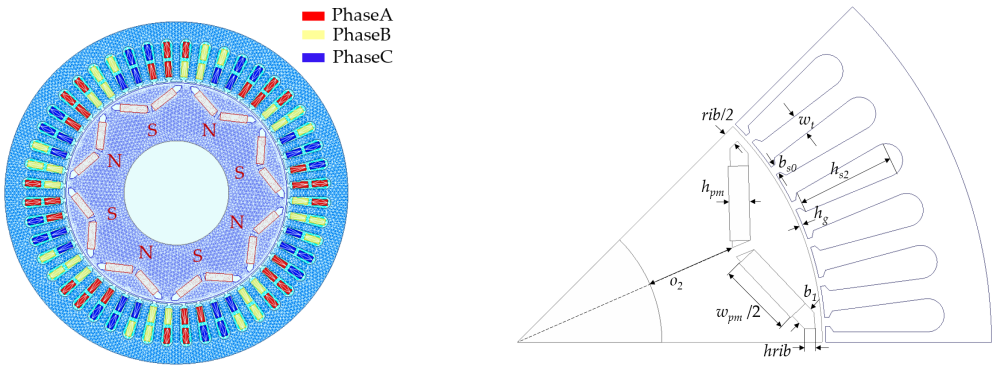

(**a**) (**b**)

Figure 1. Model of IPMSM: (**a**) grid partitioning; (**b**) 1/8 parameterization model.

Table 1. Primary parameters of the IPMSM.

Parameter	Unit	Value
Rated speed	rpm	3000
Rated power	kW	30
Rated voltage	V	336
Stator outer radius	mm	210
Stator inner radius	mm	136.5
Rotor outer radius	mm	135
Axial length	mm	210
PM	-	NdFe35
Number of poles/slots	-	8/48

The flowchart of the multi-objective optimization method of the motor proposed in this paper is shown in Figure 2. The optimization steps are present as follows:

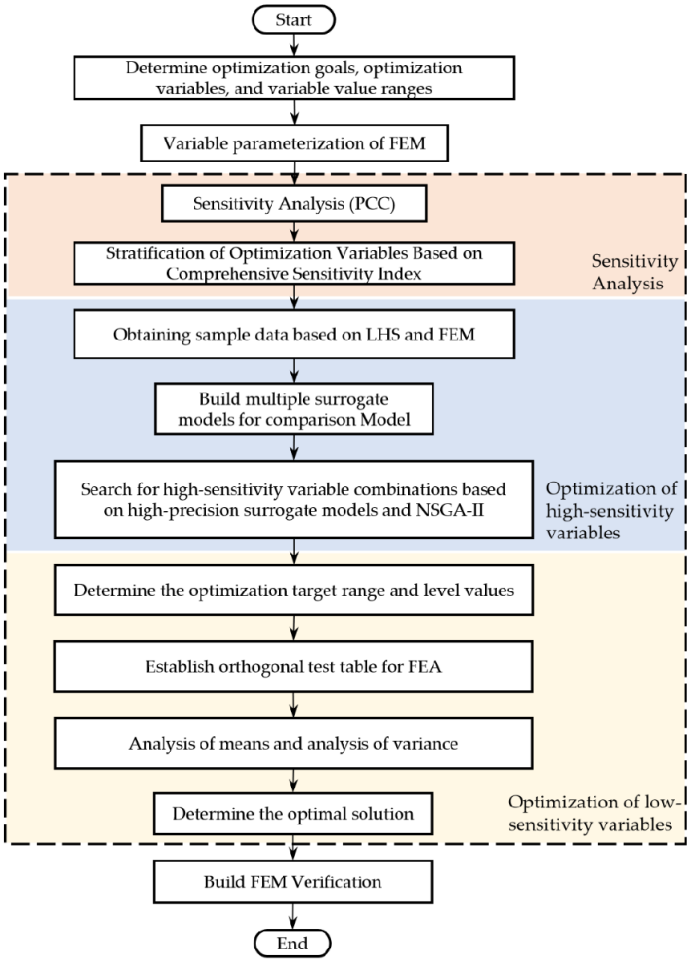

Figure 2. Flowchart of multi-objectives optimization method.

① Determining the optimization objectives and variables and establishing the parameterization model of the motor through parameterization settings.
② Performing subsequent optimizations by dividing the optimization variables into two layers of high-sensitivity and low-sensitivity according to the sensitivity value of the optimization variables toward the optimization objectives.
③ Obtaining sample datasets by using LHS and FEM for high-sensitivity optimization variables and then constructing a high-precision surrogate model based on the sample datasets.

④ Obtaining the optimal combination of high-sensitivity optimization variables based on the high-precision surrogate model and NSGA-II and optimizing the low-sensitivity optimization variables with the Taguchi method.
⑤ Evaluating the performances of the initial and optimized motors.

3. Multi-Objective Optimization of IPMSM

3.1. Determination of Optimization Variables and Optimization Objectives

3.1.1. Determination of Optimization Objectives

An electromagnetic (EM) torque is one of the vital performance indicators of the IPMSM, and the interaction of the magnetic field around the IPMSM stator current and the PM generates an electromagnetic torque. During the operation of the IPMSM, the value of the EM torque is not constant and fluctuates around the average torque. The degree of fluctuation can be expressed by torque ripple. The torque ripple is a ratio of the difference between the maximum peak value and the minimum peak value of the electromagnetic torque to the average torque. During motor operation, as the torque ripple increases, the vibration of the motor increases, and stability decreases. The calculation equation of the electromagnetic torque and the torque ripple can be expressed as [27]:

$$T_{em} = \frac{3}{2} p \left[\psi_f i_q + (L_d - L_q) i_d i_q \right] \tag{1}$$

$$T_a = avg(T_{em}) \tag{2}$$

$$T_r = \frac{T_{em\_\max} - T_{em\_\min}}{T_a} \times 100\% \tag{3}$$

where T_{em} is the electromagnetic torque; p is the polar logarithm; ψ_f is the PM chain; L_d and L_q are the d-axis and q-axis inductances of the motor, respectively; and i_d and i_q are the d-axis and q-axis currents of the motor, respectively. $T_{em\_\max}$ is the maximum peak value of the electromagnetic torque, and $T_{em\_\min}$ is the minimum peak value of the electromagnetic torque.

In the process of electromechanical energy conversion within the IPMSM, there should be a certain loss that includes copper loss, iron loss, PM eddy current loss, and additional loss, among which iron loss and copper loss are dominated. Over-loss leads to a reduction in motor efficiency and an increase in temperature, so it is significant to reduce the loss during the operation of the motor. Based on the above analysis, average torque, torque ripple, iron loss, and copper loss of the motor are selected as the optimization objectives. The iron loss of the motor can be expressed as [28]:

$$p_{fe} = p_h + p_c + p_a = k_h f B_m^{\alpha} + k_c f^2 B_m^2 + k_a f^{1.5} B_m^{1.5} \tag{4}$$

where p_h is the hysteresis loss, p_c is the eddy current loss, p_a is the abnormal eddy current loss, B_m is the magnetic density amplitude of the iron core, f is the frequency, k_h is the hysteresis loss coefficient, k_a is the abnormal eddy current loss coefficient, and α is the Stamets coefficient.

The copper loss p_{Cu} of the IPMSM can be expressed as [29]:

$$p_{Cu} = mI^2R \tag{5}$$

where m is the number of phases, I is the effective value of the phase current, and R is the phase resistance.

3.1.2. Selection of Optimization Variables

As shown in Figure 1b, the installation position of PM in the core of the motor rotor depended on the dimensions of h_{pm}, w_{pm}, rib, $hrib$, o_2, and b_1. Changes in the usage and position of the PM cause changes in the internal magnetic field intensity distribution of the motor, thus affecting the output torque performance of the motor. The stator b_{s0} in

the iron core of the stator has a great impact on the air gap magnetic conductance of the motor, which affects the tooth groove torque of the motor. The tooth groove torque causes the motor to vibrate and run unstably, which is one of the main causes of excessive torque ripple, so optimizing b_{s0} can play a role in suppressing the torque ripple of the motor. The area of each groove in the iron core of the stator is mainly determined by w_t and h_{s2}. Changes in w_t and h_{s2} affect the magnetic field distribution of the teeth and the yoke of the stator. Therefore, it has a great and certain impact on the iron loss and the copper loss, respectively, during the motor operation. On the other hand, the conversion efficiency of electromechanical energy is mainly affected by the air gap dimension between the outer surface of the rotor and the inner surface of the stator. Therefore, the length of the air gap is a crucial dimension and has a significant impact on the performance of the motor. Based on the above analysis, the structural parameters of h_{s2}, b_{s0}, w_t, h_g, rib, w_{pm}, o_2, b_1, $hrib$, and h_{pm} were selected as the variables for this optimization. The value range for each variable is presented in Table 2. To facilitate the subsequent change in the structural parameters of the motor, it is necessary to parameterize the relevant structural parameters in the FEM of the motor and as shown in Figure 1b.

Table 2. Initial values and value ranges for optimization variables.

Symbolic Representation	Initial Value (mm)	Value Range (mm)
h_{s2}	21	18–24
h_{pm}	4.5	4–5
b_{s0}	2	1.5–3
w_t	4.53	4–5
h_g	0.75	0.5–1
o_2	20	18–22
b_1	4	3.5–4
rib	6	5–7
$hrib$	2.4	2–3
w_{pm}	33	32–36

3.2. Sensitivity Analysis

Because the number of optimization variables is up to 10, if the polynomial fitting or the surrogate model is used to construct the functional relationship of these ten optimization variables and the optimization objectives simultaneously, it is not easy to ensure that the surrogate model has enough fitting quality. In particular, some non-sensitive optimization variables are easily ignored. Moreover, multi-objective optimization algorithms require more computational time when dealing with many optimization variables, even if it is difficult to converge. Therefore, it is necessary to reduce the dimensionality of the optimization variables. The original ten optimization variables are divided into two groups with low and high sensitivity. To rationally allocate the combination of the optimization variables, it is necessary to analyze the sensitivity of each optimization variable to the optimization objective and allocate the sensitivity of the optimization objectives according to the optimization variables. The sensitivity analysis step is as follows: First, the input variables (optimization variables) and the output objectives (optimization objectives) are determined, Secondly, sampling the input variable by the sample extraction method DOE (Design of Experiment). Then, the output objectives of the corresponding samples are obtained based on FEA. Finally, the sensitivities of each variable to the output objectives are calculated.

The value ranges for optimization variables are shown in Table 2. Since the motor is a strongly coupled, non-linear complex system, it is necessary to consider the interaction between the variables when sampling the sample points. In the sampling process, if a simple random sampling (SRS) method is used to sample the variables within the value ranges, the previously generated samples are not considered when developing each new model, which has large randomness and uncertainty and may not be able to obtain uniformly distributed

samples. Therefore, a stratified sampling technique LHS [30] is introduced, and the specific implementation steps are as follows:

① Distributing the range of the value for each variable into n intervals of the same length.
② Taking only one sample in each interval of each variable and taking the samples in each interval at random.
③ Randomly combining the samples sampled in step ②.

There are some variables in the IPMSM, and minor changes in these variables will have an enormous impact on the performance of the motor. Therefore, the number of samples in this sampling is selected as 100, ensuring that the distance between adjacent samples drawn for each variable is small enough. After LHS processing, the samples are sufficiently representative to consider the interaction between the variables adequately.

After obtaining a uniformly distributed sample, the output value of each sample is calculated by FEA. Then the Pearson correlation coefficient (PCC) is used to reflect the degree of sensitivity between the optimization variable and the optimization objective. The value of the PCC ranges from -1 to 1. When the PCC is greater than 0, it indicates a positive correlation between the optimization variable and the optimization objective. When the PCC is less than 0, it indicates a negative correlation between the optimization variable and the optimization objective. The absolute value of the PCC closer to 1 indicates that there is a strong correlation, and the PCC's calculation equation is:

$$\rho(X,Y) = \frac{COV(X,Y)}{\sigma_X \sigma_Y} \tag{6}$$

where *COV (X, Y)* is the covariance of the optimization variable X, and the optimization objective Y, $\sigma_{X,}$ and σ_Y are the standard deviations of X and Y, respectively.

The sensitivity of each optimization variable to the optimization objective is calculated according to Equation (6), and the results are shown in Figure 3. Each optimization variable is different for the PCC of the different optimization objectives. For instance, the optimization variables with a significant impact on T_r are b_{s0}, w_t, h_g, *rib*, and w_{pm}. The optimization variables with an enormous impact on p_{Cu} are h_{s2} and w_t. The optimization variables with a significant impact on T_a are b_{s0}, w_t, *and* w_{pm}. The optimization variables with an enormous impact on p_{fe} are h_{s2}, w_t, and h_g. Based on the above analysis, the optimization variables that have a significant effect on each optimization objective are not identical, and it is impossible to select the key optimization variables. Therefore, it is necessary to study the sensitivity of each optimization variable as follows:

$$Sen_c(x_i) = \omega_1 |S_{T_a}(x_i)| + \omega_2 |S_{T_r}(x_i)| + \omega_3 \left| S_{p_{fe}}(x_i) \right| + \omega_4 \left| S_{p_{Cu}}(x_i) \right| \tag{7}$$

where x_i is the optimization variable; $S_{Ta}(x_i)$, $S_{Tr}(x_i)$, $S_{pfe}(x_i)$, and $S_{pCu}(x_i)$ are the sensitivity values of x_i to T_a, T_r, p_{fe}, and p_{Cu}, respectively; Sen_c (x_i) is the comprehensive sensitivity of the optimization variable x_i; ω_1, ω_2, ω_3, and ω_4 are the weight coefficients of average torque, torque ripple, iron loss, and copper loss, respectively; and $\omega_1 + \omega_2 + \omega_3 + \omega_4 = 1$. In this stage, setting the weighting ratio of torque performance and losses to 0.6:0.4, $\omega_1 = \omega_2 = 0.3$, $\omega_3 = \omega_4 = 0.2$. The composite sensitivity value of each optimization variable is studied from Equation (7) and as shown in Table 3. Stratification is performed according to the comprehensive sensitivity values of the optimization variables. Using the stratified optimization strategy can greatly improve optimization accuracy and efficiency. First, the optimization variables are sorted in the order of the comprehensive sensitivity from high to low. The first six optimization variables are classified as high-sensitivity variables, and the remaining ones are classified as low-sensitivity variables. The final high-sensitivity optimization variables are h_{s2}, b_{s0}, w_t, h_g, *rib*, and w_{pm}. The low-sensitivity ones are o_2, b_1, *hrib*, and h_{pm}.

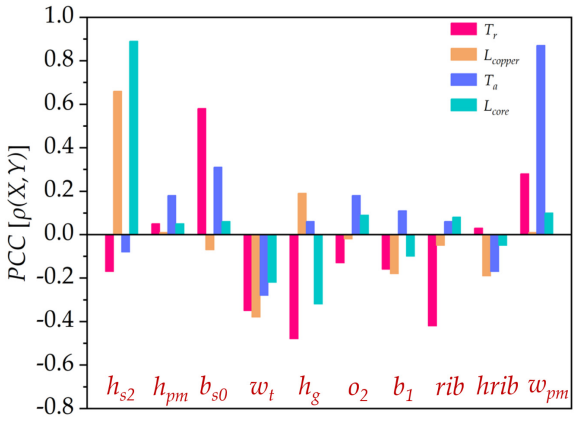

Figure 3. Sensitivity of optimization variables and optimization objectives.

Table 3. Comprehensive sensitivity values of optimization variables.

Variables	S_{Ta} (x_i)	S_{Tr} (x_i)	S_{pfe} (x_i)	S_{pCu} (x_i)	Sen_c (x_i)
h_{s2}	−0.08	−0.17	0.89	0.66	0.39
h_{pm}	0.18	0.05	0.05	0.01	0.08
b_{s0}	0.31	0.58	0.06	−0.07	0.29
w_t	−0.28	−0.35	−0.22	−0.38	0.31
h_g	0.06	−0.48	−0.32	0.19	0.26
o_2	0.18	−0.13	0.09	−0.02	0.12
b_1	0.11	−0.16	−0.1	−0.18	0.14
rib	0.06	−0.42	0.08	−0.05	0.17
$hrib$	−0.17	0.03	−0.05	−0.19	0.11
w_{pm}	0.87	0.28	0.1	0.01	0.37

3.3. Establishment of the Surrogate Model

In the high-dimensional, non-linear optimization problem, if the parametric scanning method or evolutionary algorithm is directly employed to search within the value ranges of the optimization variable, thousands of FEMs need to be built and calculated with huge time and costs. Therefore, we used the high-precision surrogate model to fit the complex relationship between the optimization variables and the optimization objectives. As a result, there is no need for many data samples to simulate a similar simulation model, which significantly improves the optimization efficiency.

To obtain a more accurate surrogate model, in this paper, six regression prediction algorithms, including (1) back propagation (BP), (2) Kriging, (3) convolutional neural network (CNN), (4) random forest (RF), (5) support vector regression (SVR), and (6) extreme gradient boosting (XGboost) are used to construct the surrogate model of optimization variables and optimization objectives. The settings of the BP neural network are: the number of layers of the BP neural network is 3. The number of neurons in the input layer is 6, the number of hidden layers is 1, and the number of neurons in each hidden layer is 5. The number of neurons in the output layer is 1. The settings of CNN are: the input layer of CNN is set to [6 1 1], the number of convolutional layers is 1, the size of the convolutional kernel is set to [3 1], and the number of convolutional kernels is 16. The activation function used in the activation layer is ReLU. The filter of the pooling layer is set to [2 1], and the step size is 2. The number of neurons in the fully connected layer is 384, and the number of neurons in the output layer is 1. Then, the evaluation indicators under the two groups of normalization and non-normalization of sample points are calculated, respectively. The total number of datasets is 300, and the dataset is divided into a training set and a test set with a ratio of 8:2. The accuracy of the surrogate models are compared by calculating the evaluation indicators. Commonly used regression model evaluation indicators are coefficient of determination (R^2), root mean square error ($RMSE$), mean absolute error

(*MAE*), mean square error (*MSE*), mean absolute percentage error (*MAPE*), and symmetric mean absolute percentage error (*SMAPE*), where *RMSE*, *Mae*, and *MSE* cannot reflect the goodness of the model when the selection range of multiple objective functions has a big difference. Therefore, the most suitable surrogate model is selected from the R^2, *MAPE*, and *SMAPE* of the main comparison models. R^2 is the evaluation indicator that best reflects the degree of fit. The closer R^2 to 1, the better the fitting. On the other hand, the smaller *MAPE* and *SMAPE*, the better the effect of the predictive model. The calculation of indicators of these three regression evaluations can be expressed as follows:

$$R^2 = 1 - \frac{\sum_{i=1}^{n} \left(y_i - \hat{y_i}\right)^2}{\sum_{i=1}^{n} \left(y_i - \bar{y}\right)^2} \tag{8}$$

$$MAPE = \frac{100\%}{n} \sum_{i=1}^{n} \left| \frac{y_i - \hat{y_i}}{y_i} \right| \tag{9}$$

$$SMAPE = \frac{100\%}{n} \sum_{i=1}^{n} \frac{|\hat{y_i} - y_i|}{(|\hat{y_i}| + |y_i|)/2} \tag{10}$$

where n is the number of samples in the test set, y_i is the actual values of the samples of the test set, $\hat{y}_i$ is the predicted values of the samples of the test set, and $\bar{y}$ is the average value of the actual values of the samples of the test set. The test results of each surrogate model are shown in Figures 4 and 5, and the specific evaluation indicators are shown in Table 4.

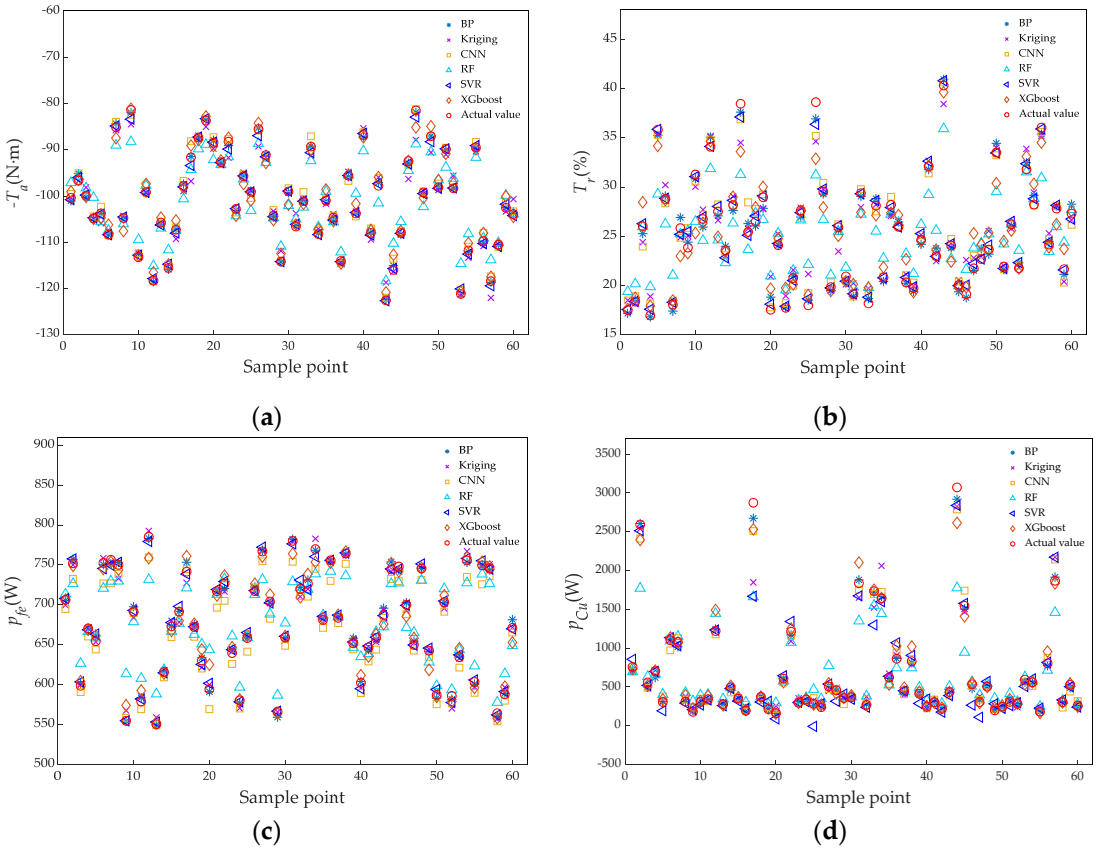

Figure 4. Prediction results of normalization of sample points: (**a**) test results of $-T_a$; (**b**) test results of T_r; (**c**) test results of p_{fe}; (**d**) test results of p_{Cu}.

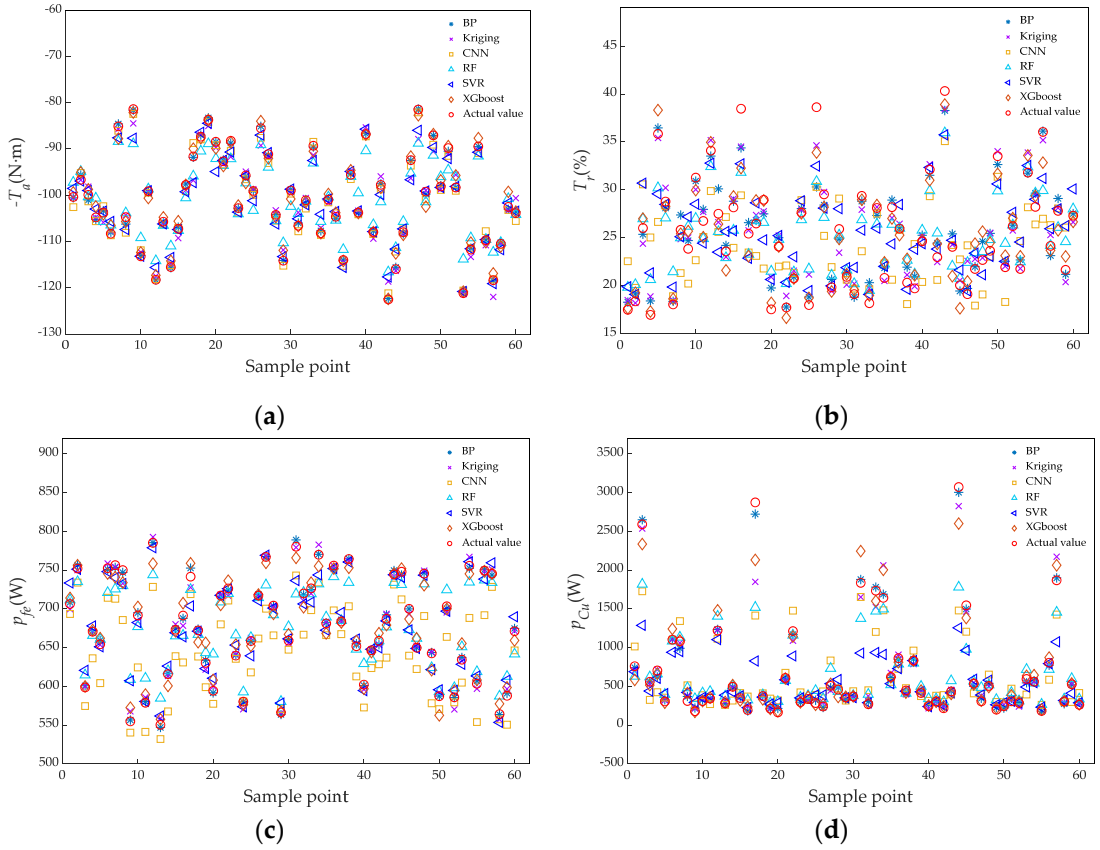

Figure 5. Prediction results of no normalization of sample points: (**a**) test results of $-T_a$; (**b**) test results of T_r; (**c**) test results of p_{fe}; (**d**) test results of p_{Cu}.

Table 4. Evaluation indicators of each surrogate model.

Surrogate Model	Evaluating Indicator	Optimization Objective							
		Normalization of Sample Data				No Normalization of Sample Data			
		$-T_a$	T_r	p_{fe}	p_{Cu}	$-T_a$	T_r	p_{fe}	p_{Cu}
BP	*MAPE* (%)	0.310	2.155	0.473	3.504	**0.308**	4.179	**0.342**	**6.038**
	SMAPE (%)	0.310	2.152	0.473	3.552	**0.308**	4.157	**0.341**	**5.832**
	R^2	0.998	0.988	0.996	0.996	**0.998**	0.923	**0.998**	**0.997**
Kriging	*MAPE* (%)	1.471	4.483	0.779	10.400	1.471	4.483	0.779	10.400
	SMAPE (%)	1.459	4.400	0.781	9.846	1.459	4.400	0.781	9.846
	R^2	0.963	0.938	0.990	0.940	0.963	0.938	0.990	0.940
CNN	*MAPE* (%)	0.824	2.921	1.856	10.757	1.113	13.347	5.041	31.017
	SMAPE (%)	0.828	2.898	1.877	10.419	1.109	13.678	5.206	28.501
	R^2	0.990	0.971	0.953	0.981	0.983	0.491	0.721	0.727
RF	*MAPE* (%)	2.684	8.386	2.767	21.774	2.886	8.314	2.675	25.023
	SMAPE (%)	2.668	8.370	2.759	19.671	2.867	8.248	2.671	22.27
	R^2	0.908	0.782	0.881	0.805	0.892	0.788	0.887	0.794
SVR	*MAPE* (%)	0.478	**1.538**	0.522	16.424	1.668	8.831	1.721	21.093
	SMAPE (%)	0.476	**1.529**	0.521	19.178	1.652	8.718	1.721	22.137
	R^2	0.996	**0.991**	0.996	0.915	0.951	0.773	0.944	0.540
XGboost	*MAPE* (%)	1.243	5.200	1.214	7.315	1.064	5.157	1.512	8.581
	SMAPE (%)	1.244	5.200	1.213	7.064	1.067	5.173	1.513	8.447
	R^2	0.979	0.895	0.975	0.975	0.983	0.908	0.967	0.946

In Table 4, the prediction accuracy of all the surrogate models except the Kriging model for the same optimization objective differs under normalized and non-normalized conditions for the training samples. The R^2 values of each surrogate model for the optimization target were compared, and the largest one was selected. If the R^2 is the same, compare MAPE and SMAPAE and select the smallest. After the comparison, the BP neural network agent model has the highest prediction accuracy for p_{Cu}, p_{fe}, and $-T_a$ under the unnormalized condition of the training samples is obtained. The SVR agent model has the highest prediction accuracy for T_r under the normalized condition of the training samples. There are the bolded parts in Table 4. Therefore, the BP neural network model and the SVR ones are adopted to construct the surrogate model of the optimization variables and the objectives.

3.4. Multi-Objective Optimization of IPMSM Based on NSGA-II and Taguchi Method

3.4.1. Optimization of High-Sensitivity Variables

When combined with the high-precision surrogate model established above, the optimal combination of design parameters is searched by using a multi-objective optimization algorithm. NSGA-II is widely used in multi-objective optimization problems due to its fast speed and strong searchability. Therefore, in this paper, the optimal combination of design parameters of the IPMSM is searched by NSGA-II. The specific implementation steps are shown in Figure 6.

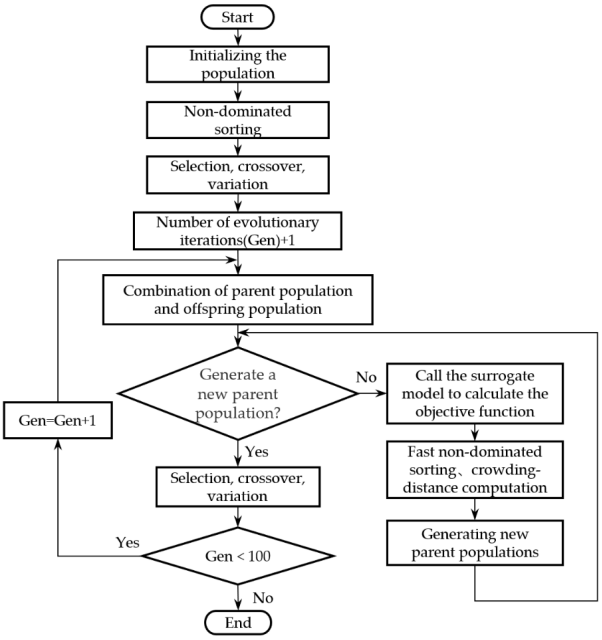

Figure 6. Optimization flowchart of NSGA-II.

The objective function is defined as:

$$\min : \begin{cases} f_1(x) = -T_a \\ f_2(x) = T_r \\ f_3(x) = p_{fe} + p_{Cu} \end{cases} \tag{11}$$

where x is the optimization variable, and the value ranges of the optimization variables are shown in Table 2. The constraint conditions are $-T_a$, T_r, and $p_{fe} + p_{Cu}$, which are smaller than the $-T_a$, T_r, and $p_{fe} + p_{Cu}$ of an initial motor, respectively:

$$\begin{cases} c_1(x) = -T_a + 91.34 < 0 \\ c_2(x) = T_r - 22.13\% < 0 \\ c_3(x) = p_{fe} + p_{Cu} - 970 < 0 \end{cases} \tag{12}$$

The Pareto solution set is obtained according to the above settings and methods, as shown in Figure 7. It can be seen that optimization objectives $f_1(x)$, $f_2(x)$, and $f_3(x)$ cannot all obtain optimal values simultaneously. To make a reasonable compromise on the three optimization objectives, four candidate points in the middle are selected for comparison according to the order of the average torque. In Table 5, candidate point 3 is the optimal one of the four candidate points. Therefore, candidate point 3 is selected as the final value of the high-sensitivity variable, as shown in a five-pointed star point in Figure 7.

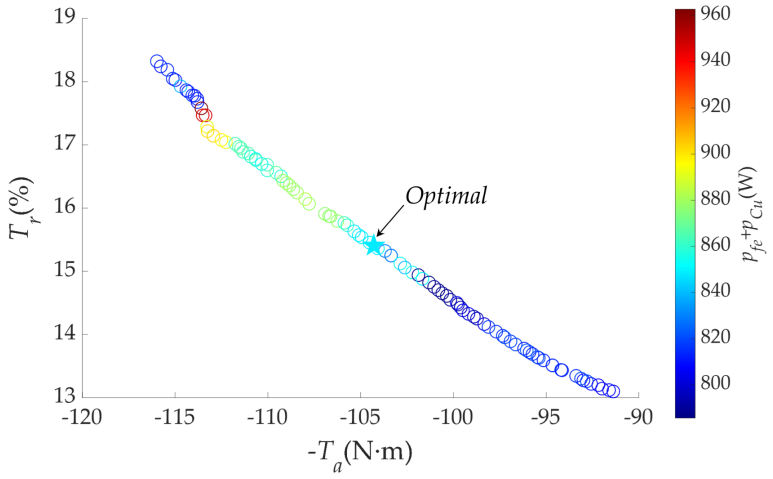

Figure 7. Pareto solution after NSGA−II optimization.

Table 5. Optimal candidate solutions.

	h_{s2} (mm)	b_{s0} (mm)	w_t (mm)	h_g (mm)	*rib* (mm)	w_{pm} (mm)	$-T_a$ (N·m)	T_r (%)	p_{fe} + p_{Cu} (W)
Candidate Point1	19.31	1.87	4.75	1	7	34.55	−104.94	15.54	849.05
Candidate Point2	19.3	1.88	4.75	1	7	34.49	−104.52	15.45	849.16
Candidate Point3	19.3	1.88	4.75	1	7	34.47	−104.29	15.4	848.43
Candidate Point4	19.31	1.89	4.75	1	7	34.43	−104.07	15.36	849.62

3.4.2. Optimization of Low-Sensitivity Variables

After the high-sensitivity optimization variables are optimized, the next step is to optimize the low-sensitivity optimization variables. Since the overall impact of the low-sensitivity optimization variables on the optimization objectives is low, the optimization enhancement space is small. Therefore, the Taguchi optimization method with strong local search ability is adopted to optimize the low-sensitivity optimization variables and save computation time. The new FEM is established according to the combination of variables obtained after NSGA-II optimization. Then, the Taguchi method is used to optimize the four low-sensitivity optimization variables of o_2, b_1, *hrib*, and h_{pm}. First, the value ranges and the values of the level of the optimization variables are determined. Taking 3 level values for this optimization, the spacing between level values is equal. Each level value is named level 1, level 2, and level 3, from small to big, respectively. The specific values are shown in Table 6.

Table 6. Level values of optimization variables.

Optimization Variables	Level 1	Level 2	Level 3
o_2	18	20	22
b_1	3.5	3.75	4
hrib	2	2.5	3
h_{pm}	4	4.5	5

According to the results in Table 6, The L_9 (3^4) orthogonal test table is established and as shown in Table 7. Then, the corresponding FEM is established to calculate the four objective values.

Table 7. L_9 (3^4) orthogonal test table and FEA results.

Number of Tests	o_2	b_1	*hrib*	h_{pm}	T_a (N·m)	T_r (%)	$p_{fe} + p_{Cu}$ (W)
1	1	1	1	1	90.09	17.63	854.93
2	1	2	2	2	95.86	17.36	860.83
3	1	3	3	3	100.55	17.27	866.7
4	2	1	2	3	99.63	17.46	865.45
5	2	2	3	1	90.72	18.32	854.47
6	2	3	1	2	106.94	13.81	879.01
7	3	1	3	2	92.29	18.56	857.01
8	3	2	1	3	110.46	15.00	883.67
9	3	3	2	1	99.45	16.13	866.43

According to the established orthogonal test Table 7, the average value is analyzed, and the objective average value of each variable under different level values is calculated, as shown in Figure 8. It shows that the most favorable combination of variables for increasing T_a is o_2 (3) b_1 (3) *hrib* (1) h_{pm} (3). The most favorable combination of variables for decreasing *Tr* is o_2 (2) b_1 (3) *hrib* (1) h_{pm} (2) or o_2 (2) b_1 (3) *hrib* (1) h_{pm} (3). That for decreasing $p_{fe} + p_{Cu}$ is o_2 (1) b_1 (1) *hrib* (3) h_{pm} (1). The combinations of T_a, T_r, and $p_{fe} + p_{Cu}$ are not the same under optimal conditions. Therefore, the data in Table 7 need to be analyzed for variance. The variance calculation equation can be expressed as:

$$\bar{n} = \frac{1}{m}\sum_{k=1}^{m} n_k \tag{13}$$

$$S^2_{n(x)} = \frac{1}{L}\sum_{i=1}^{L}\left(n(x)_i - \bar{n}\right)^2 \tag{14}$$

where $\bar{n}$ is the total average value of the optimization objective n, m is the total number of trials, $S^2{}_{n(x)}$ is the variance of the optimization objectives n (x), L is the level number, and $n(x)_i$ is the objective average value when the variable x is at level i.

The variance values and proportion of variables with respect to the optimization objectives were calculated according to Equations (13) and (14) and Table 7, as shown in Table 8.

According to the comparison of the proportion values in Table 8, the rate of the impact of o_2 on $p_{fe} + p_{Cu}$ is the largest. The rate of the impact of b_1 on T_r is the largest. The rate of the impact of *hrib* on T_r is the largest, and the rate of the impact of h_{pm} on T_a is the largest. Therefore, o_2 (1) b_1 (3) *hrib* (1) h_{pm} (3) is selected as the optimal combination, and the values of motor variables optimized by the Taguchi method are shown in Table 9.

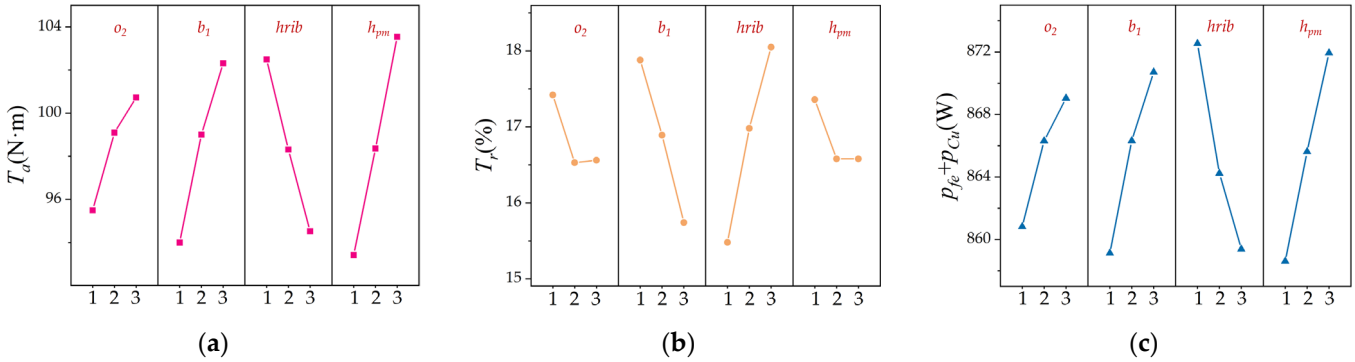

Figure 8. Impact of level values of optimization variables on optimization objectives: (**a**) impact of variable level on T_a; (**b**) impact of variable level on T_r; (**c**) impact of variable level on $p_{fe} + p_{Cu}$.

Table 8. Variance values and proportion between optimization variables and optimization objectives.

Variables	$S^2_{T_a}$	Proportion (%)	$S^2_{T_r}$ ($\times 10^{-5}$)	Proportion (%)	$S^2_{p_{fe}+p_{Cu}}$	Proportion (%)
o_2	4.78	10.82	1.70	7.77	11.68	12.48
b_1	11.67	26.43	7.70	35.21	22.80	24.36
$hrib$	10.61	24.03	11.11	50.80	29.46	31.48
h_{pm}	17.10	38.72	1.36	6.22	29.64	31.67

Table 9. Design variables for the initial and optimized motors.

Classification of Variables	Variable	Initial	BP + SVR + NSGA-II	BP + SVR + NSGA-II + Taguchi
High sensitivity variables	h_{s2}	21	19.3	19.3
	b_{s0}	2	1.88	1.88
	w_t	4.53	4.75	4.75
	h_g	0.75	1	1
	rib	6	7	7
	w_{pm}	33	34.47	34.47
Low sensitivity variables	o_2	20	20	18
	b_1	4	4	4
	$hrib$	2.4	2.4	2
	h_{pm}	4.5	4.5	5

4. Results and Discussions

In order to verify the effectiveness of the above optimization methods, the performance of the variable-optimized motor was analyzed by finite element analysis (FEA) and compared to that of the optimized motor. Figure 9a shows the electromagnetic (EM) torque of the initial IPMSM and the optimized ones in the time domain. Figure 9b shows the iron losses of the initial IPMSM and the optimized ones. Figure 9c shows the copper losses of the initial IPMSM and the optimized ones. More detailed performance parameters of the initially designed motor and optimally designed ones with different methods are shown in Table 10.

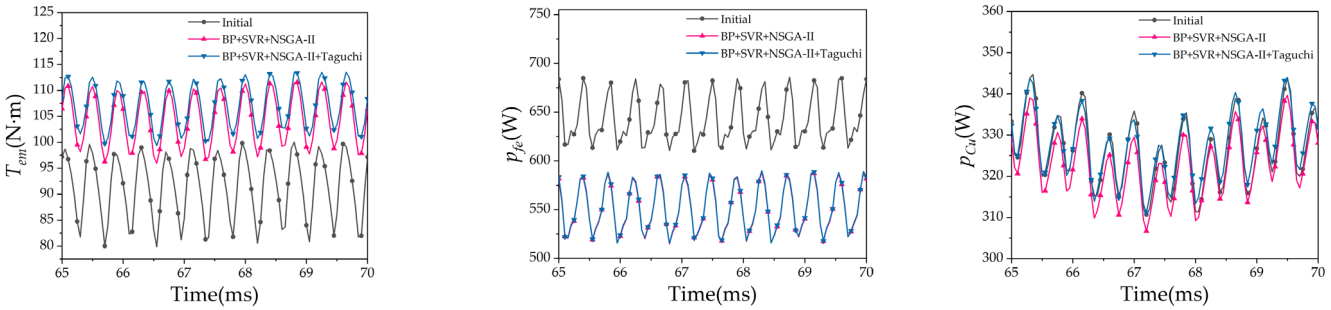

Figure 9. Performance comparison of the initial motor and the optimized motor: (**a**) comparison of T_a; (**b**) comparison of p_{fe}; (**c**) comparison of p_{Cu}.

Table 10. Performance comparison of initial motor and optimized motor with different optimization methods.

Performance	Initial	BP + SVR+ NSGA-II	BP + SVR + NSGA-II + Taguchi
T_a (N·m)	91.34	104.39	**106.96**
T_r (%)	22.13	15.03	**13.23**
T_c (N·m)	6.43	5.23	**5.09**
p_{fe} (W)	643.1	551.07	551.8
p_{Cu} (W)	326.56	323.05	327.56
Efficiency (%)	93.88	94.78	**94.84**

It can be seen that after the BP + SVR + NSGA-II solution optimizes the high-sensitivity variables of the motor, the performance of the IPMSM is greatly improved, the average torque is increased by 14.29%, the torque ripple is decreased by 32.08%, the iron loss is decreased by 14.31%, the copper loss is decreased by 1.08%, and the efficiency is increased to 94.78%.

The BP + SVR + NSGA-II + Taguchi optimization scheme is proposed due to the best performance. Compared to the motor optimized by the optimization strategy in this paper with the initial IPMSM, the average torque is increased by 17.1%, the torque ripple is reduced by 40.22%, the iron loss is reduced by 14.2%, the change in copper loss is very small, and the efficiency is increased to 94.84%.

5. Conclusions

In this paper, we propose a multi-objective optimization strategy for IPMSMs based on BP + SVR combined surrogate model with NSGA-II + Taguchi method. The average torque, torque ripple, iron loss, and copper loss of the IPMSM are used as optimization objectives to optimize the IPMSM. The verification of the numerical calculation results shows that the surrogate model constructed in this paper has very high accuracy, and the prediction results of each optimization objective have very small errors with the numerical calculation results. Compared with the performance of the initial design motor and optimized ones by other optimization strategies, the results show that the overall performance of IPMSM optimized by our proposed multi-objective optimization strategy is best. In the future, we will build the physical motor based on the results obtained in this paper to verify the effectiveness of our proposed method.

Author Contributions: Conceptualization, Y.Y. and Y.P.; methodology, Y.Y.; software, Y.P.; writing original draft, Y.Y. and Y.P. writing—review and editing, Y.Y., J.G., Q.C., Y.H., J.G., Z.Z., S.N. and S.Z. All authors have read and agreed to the published version of the manuscript.

Funding: This research was supported in part by the National Natural Science Foundation of China (Grant No. 52067006, 52162044)), in part by the Foreign expert Bureau of the Ministry of science and

technology of China (Grant No. G2021022002L), in part by long-term project of innovative leading talents in the "Double Thousand Plan" of Jiangxi Province (jxsq2019101027).

Data Availability Statement: Not applicable.

Acknowledgments: The authors would like to thank anonymous reviewers for their helpful comments and suggestions to improve the manuscript.

Conflicts of Interest: The authors declare no conflict of interest.

References

1. Guo, Y.; Si, J.; Gao, C. Improved Fuzzy-Based Taguchi Method for Multi-Objective Optimization of Direct-Drive Permanent Magnet Synchronous Motors. *IEEE Trans. Magn.* **2019**, *55*, 1–4. [CrossRef]
2. Zheng, J.Q.; Zhao, W.X.; Ji, J.H.; Li, H.T. Review on Design Methods of Low Harmonics of Fractional-slot Concentrated-windings Permanent-magnet Machine. *Proc. CSEE* **2020**, *40*, 272–280.
3. Zheng, S.; Zhu, X.; Xu, L. Multi-Objective Optimization Design of a Multi-Permanent-Magnet Motor Considering Magnet Characteristic Variation Effects. *IEEE Trans. Ind. Electron.* **2022**, *69*, 3428–3438. [CrossRef]
4. Zheng, L.; Yu, X.Z.; Wang, X.T.; Xing, X.X. Optimization and Analysis of Cogging Torque of Permanent Magnet Spherical Motor. *IEEE Trans. Appl. Supercond.* **2021**, *31*, 1–5.
5. Hao, L.; Lin, M.; Xu, D. Cogging torque reduction of axial-field flux-switching permanent magnet machine by rotor tooth notching. *IEEE Trans. Magn.* **2015**, *51*, 1–4.
6. Li, Z.; Yu, X.; Zhao, L. Multi-objective optimization of control parameters of deflectable dual-stator switched reluctance generator at low speed. *Electr. Eng.* **2022**, *104*, 2397–2406. [CrossRef]
7. Zhang, Q.; Cheng, S.; Wang, D. Multiobjective design optimization of high-power circular winding brushless DC motor. *IEEE Trans. Ind. Electron.* **2017**, *65*, 1740–1750.
8. Gao, F.Y.; Gao, J.N.; Li, M.M.; Yao, P.; Song, Z.X.; Yang, K.W.; Gao, X.Y. Optimization Design of Halbach Interior Permanent Magnet Synchronous Motor Based on Parameter Sensitivity Stratification. *J. Xi'an Jiaotong Univ.* **2022**, *56*, 180–190.
9. Husain, T.; Hasan, I.; Sozer, Y. Cogging torque minimization in transverse flux machines. *IEEE Trans. Ind. Appl.* **2018**, *55*, 385–397. [CrossRef]
10. Karimpour, S.R.; Besmi, M.R.; Mirimani, S.M. Optimal design and verification of interior permanent magnet synchronous generator based on FEA and Taguchi method. *Int. Trans. Electr. Energy Syst.* **2020**, *30*, e12597. [CrossRef]
11. Cho, S.-K.; Jung, K.-H.; Choi, J.-Y. Design Optimization of Interior Permanent Magnet Synchronous Motor for Electric Compressors of Air-Conditioning Systems Mounted on EVs and HEVs. *IEEE Trans. Magn.* **2018**, *54*, 1–5. [CrossRef]
12. Sun, X.; Shi, Z.; Zhu, J. Multiobjective design optimization of an IPMSM for EVs based on fuzzy method and sequential taguchi method. *IEEE Trans. Ind. Electron.* **2020**, *68*, 10592–10600. [CrossRef]
13. Shi, Z.; Sun, X.; Cai, Y. Robust design optimization of a five-phase PM hub motor for fault-tolerant operation based on Taguchi method. *IEEE Trans. Energy Convers.* **2020**, *35*, 2036–2044. [CrossRef]
14. Zhu, H.; Shen, S.; Wang, X. Multiobjective Optimization Design of Outer Rotor Coreless Bearingless Permanent Magnet Synchronous Motor. *IEEE J. Emerg. Sel. Top. Power Electron.* **2021**, *9*, 5489–5498. [CrossRef]
15. Chen, Y.Y.; Zhu, X.Y.; Quan, L.; Han, X.; He, X.J. Parameter Sensitivity Optimization Design and Performance Analysis of Double-Salient Permanent-Magnet Double-Stator Machine. *Trans. China Electrotech. Soc.* **2017**, *32*, 160–168.
16. Lei, G.; Zhu, J.; Guo, Y.; Liu, C.; Ma, B. A review of design optimization methods for electrical machines. *Energies* **2017**, *10*, 1962. [CrossRef]
17. Cao, Y.J.; Feng, L.L.; Mao, R.; Yu, L.; Jia, H.Y.; Jia, Z. Multi-objective Stratified Optimization Design of Axial-flux Permanent Magnet Memory Motor. *Proc. CSEE* **2021**, *41*, 1983–1992.
18. Sun, X.; Shi, Z.; Lei, G. Multi-objective design optimization of an IPMSM based on multilevel strategy. *IEEE Trans. Ind. Electron.* **2020**, *68*, 139–148. [CrossRef]
19. Gu, A.; Ruan, B.; Cao, W. A general SVM-based multi-objective optimization methodology for axial flux motor design: YASA motor of an electric vehicle as a case study. *IEEE Access* **2019**, *7*, 180251–180257. [CrossRef]
20. Tong, W.M.; Ma, X.J.; Wei, H.Y.; Wu, S.N. Multi objective optimization design of axial flux permanent magnet motor based on magnetic field analytical model and genetic algorithm. *Electr. Mach. Control.* **2022**, *26*, 39–45.
21. Lee, J.H.; Kim, J.W.; Song, J.Y. Distance-based intelligent particle swarm optimization for optimal design of permanent magnet synchronous machine. *IEEE Trans. Magn.* **2017**, *53*, 1–4. [CrossRef]
22. Hao, J.; Suo, S.; Yang, Y. Optimization of torque ripples in an interior permanent magnet synchronous motor based on the orthogonal experimental method and MIGA and RBF neural networks. *IEEE Access* **2020**, *8*, 27202–27209. [CrossRef]
23. Hua, Y.Z.; Liu, Y.C.; Pan, W.; Diao, X.Y.; Zhu, H.Q. Multi-Objective Optimization Design of Bearingless Permanent Magnet Synchronous Motor Using Improved Particle Swarm Optimization Algorithm [J/OL]. *Proc. CSEE* **2022**, 1–9. [CrossRef]
24. Pan, Z.; Fang, S. Combined random forest and NSGA-II for optimal design of permanent magnet arc motor. *IEEE J. Emerg. Sel. Top. Power Electron.* **2021**, *10*, 1800–1812. [CrossRef]

25. Zhu, X.; Shu, Z.; Quan, L. Multi-objective optimization of an outer-rotor V-shaped permanent magnet flux switching motor based on multi-level design method. *IEEE Trans. Magn.* **2016**, *52*, 1–8. [CrossRef]
26. Sasaki, H.; Igarashi, H. Topology optimization of IPM motor with aid of deep learning. *Int. J. Appl. Electromagn. Mech.* **2019**, *59*, 87–96. [CrossRef]
27. Zhu, X.; Huang, J.; Quan, L. Comprehensive sensitivity analysis and multiobjective optimization research of permanent magnet flux-intensifying motors. *IEEE Trans. Ind. Electron.* **2018**, *66*, 2613–2627. [CrossRef]
28. Zhang, Y.; McLoone, S.; Cao, W. Electromagnetic loss modeling and demagnetization analysis for high speed permanent magnet machine. *IEEE Trans. Magn.* **2017**, *54*, 1–5. [CrossRef]
29. Tang, R.Y. *Modern Permanent Magnet Machines: Theory and Design*; China Machine Press: Beijing, China, 2016.
30. Shields, M.D.; Zhang, J. The generalization of Latin hypercube sampling. *Reliab. Eng. Syst. Saf.* **2016**, *148*, 96–108. [CrossRef]